Verification and dosimetric impact of Acuros XB algorithm on intensity modulated stereotactic radiotherapy for locally persistent nasopharyngeal carcinoma

Monica W. K. Kan[a)]
Department of Oncology, Princess Margaret Hospital, Hong Kong SAR, China and Department of Physics and Materials Science, City University of Hong Kong, Tat Chee Avenue, Kowloon Tong, Hong Kong SAR, China

Lucullus H. T. Leung
Department of Oncology, Princess Margaret Hospital, Hong Kong SAR, China

Peter K. N. Yu
Department of Physics and Materials Science, City University of Hong Kong, Tat Chee Avenue, Kowloon Tong, Hong Kong SAR, China

(Received 11 March 2012; revised 28 May 2012; accepted for publication 18 June 2012; published 18 July 2012)

Purpose: The main aim of the current study was to assess the dosimetric impact on intensity modulated stereotactic radiotherapy (IMSRT) for locally persistent nasopharyngeal carcinoma (NPC) due to the recalculation from the Anisotropic Analytical Algorithm (AAA) to the recently released Acuros XB (AXB) algorithm. The dosimetric accuracy of using AXB in predicting air/tissue interface doses from an open single small field in a simple geometric phantom and intensity modulated small fields in an anthropomorphic phantom was also investigated.
Methods: The central axis percentage depth doses (PDD) of a rectangular phantom containing an air cavity were calculated by both AAA and AXB from 6 MV beam with small field sizes (2×2 to 5×5 cm^2). These data were compared to PDD measured by thin thermoluminescent dosimeters (TLDs) and Monte Carlo simulations. The doses predicted by AAA and AXB near air/tissue interfaces from five different IMSRT plans were compared to the TLD measured doses in an anthropomorphic phantom. The PTV coverage, conformity and doses to organs at risk (OARs) calculated by AAA and AXB were compared for 12 patients, using identical beam setup, leaves movement and monitor units.
Results: Testing using the simple rectangular phantom demonstrated that AAA and AXB overestimated the PDD at the air/tissue interfaces by up to 41% and 6%, respectively, from a 2×2 cm^2 field. The secondary build-up curves predicted by AXB caught up well with the measured data at around 2 mm beyond the air cavity. Testing using the anthropomorphic phantom showed that AAA overestimated the doses by up to 10%, while the measured doses matched those of the AXB to within 3%. Using AAA, the planning target coverage represented by 100% of the reference dose was estimated to be 4% higher than using AXB. The averaged minimum dose to the PTV predicted by AAA was about 4% higher and OARs doses 3% to 6% higher compared to AXB.
Conclusions: AXB should be used whenever possible as the standard reference for IMSRT boost of NPC cases. The more accurate AXB indicating lower target coverage and lower minimum target dose compared to AAA should be noted. © *2012 American Association of Physicists in Medicine*. [http://dx.doi.org/10.1118/1.4736819]

Key words: acuros XB algorithm, stereotactic intensity modulated radiotherapy, nasopharyngeal carcinoma, target coverage, verification

I. INTRODUCTION

Nasopharyngeal carcinoma (NPC) with local persistence after the first course of external beam radiotherapy carries a high risk of treatment failure. Persistent disease refers to the local relapse that occurs within 3–6 months after the completion of the primary radiotherapy. Linac-based stereotactic radiosurgery and radiotherapy (SRT) are shown to be effective for patients with persistent NPC.[1–3] Intensity modulated stereotactic radiotherapy (IMSRT) was shown to produce superior dose conformity, more homogeneous dose to planning target volume (PTV) while sparing more organs at risk (OARs) than other stereotactic techniques such as circular arc and static conformal beams.[4] It has been commonly used for SRT boost.

The use of IMSRT boost in NPC patients usually involves many small field segments passing through air cavities such as the nasal cavity and oral cavity. The use of small fields with the presence of air cavities always leads to the electronic disequilibrium effect near the air-tissue interfaces. This happens when the lateral range of secondary electrons becomes longer than the width of the small field segments. Heterogeneous correction is one issue that affects the dose calculation accuracy

in IMSRT planning for NPC cases. Most of the dose calculation algorithms implemented in commercially available clinical treatment planning system cannot accurately account for the electron transport near air-tissue interfaces. Algorithms such as collapsed cone convolution algorithm (CCC) and the anisotropic analytical algorithm (AAA) that apply simplified density scaling of the Monte Carlo (MC)-derived dose kernels for heterogeneous media were proved to significantly overpredict the dose near air-tissue interfaces.[5–7] A new photon dose calculation algorithm called Acuros XB (AXB) has been implemented in the Eclipse treatment planning system (Varian Medical Systems, Palo Alto, CA). AXB directly accounts for the effects of heterogeneities in patient dose calculation by explicitly solving the linear Boltzmann transport equation (LBTE) that describes the macroscopic behavior of radiation particles as they travel through and interact with matter. The development of AXB is to provide a fast and accurate alternative to the golden standard of MC calculations. With sufficient refinement, AXB can converge on the same solution of the LBTE as the MC method. Some recent investigations have shown that AXB was able to achieve comparable accuracy to MC methods in homogenous water and in heterogeneous media.[8,9,11–13] Vassiliev *et al.* proved good agreement of better than 2% between AXB and MC in a heterogeneous slab phantom and a simulated breast treatment.[8] Fogliata *et al.* compared the calculated dose distributions between AXB and MC in virtual phantoms with different materials showed good agreement at 6 and 15 MV beam using large and small fields.[12] Bush *et al.* found that the dose calculation results using AXB on a phantom containing an air cavity was within the range of 1.5%–4.5% of the MC calculated values in the tissue above and below the air cavity for a 10×10 cm^2 field at 6 MV beam.[13]

The main purpose of this study was to assess the dosimetric impact on IMSRT planning for persistent NPC due to the recalculation from AAA to AXB dose calculation method based on a group of real patient data. It is important to systematically check the accuracy of the two algorithms against experimental measured data before the assessment. The verification results in heterogeneous media previously reported were mainly performed by comparing the AXB calculated data against Monte Carlo simulated data.[8,12,13] Verification of the dose calculation accuracy of AXB version 10.0.28 (AXB10) and AAA version 10 (AAA10) for small fields (2×2–5×5 cm^2) in the presence of air cavity against measured data has not been performed. The accuracy of the older AAA version 8.6.15 (AAA8) for small fields with the presence of air cavity was investigated in our previous study.[7] The most important difference between the AAA8 and AAA10 is the refinement of fluence modeling from 2.5 mm to 0.3125 mm. Ong *et al.* found that AAA10 improved the accuracy of dose calculations compared to AAA8, and using dose calculation grid resolution of 1.0 mm was superior to using 2.5 mm.[14] The first step of our study was to compare the dose calculation accuracy of AXB10 and AAA10 against measured data and Monte Carlo simulation in a simple rectangular phantom including air cavity irradiated by 6 MV single small fields. Dose calculation accuracy of the two algorithms near air/tissue interfaces of the NP region was then compared to thermoluminescent dosimeters (TLD) measurements in an anthropomorphic phantom with actual IMSRT setups. The influence of the dose calculation grid resolution on the accuracy of AXB10 and AAA10 for small fields in the presence of air cavity was also investigated. The second stage of this study was to evaluate the change of target coverage, target conformity, and doses to OARs due to the recalculation from AAA to AXB for a group of 12 NPC patients with persistent disease.

II. METHODS AND MATERIALS

The same set of beam data used by AAA10 measured in a three-dimensional Blue Phantom (Wellhofer, IBA Dosimetry America, Bartlett, TN) for field sizes 2×2–40×40 cm^2 were imported for the configuration of AXB10. All data presented in this study were taken for a 6 MV photon beam generated from a Varian Clinac 6EX accelerator equipped with a Millennium 120 multileaf collimator (Varian Medical Systems, Palo Alto, CA). The measured data used in this work were also used by our previous study for the investigation of the accuracy of the version AAA 8.6.15.[7]

II.A. Dose calculations

The two algorithms implemented in the Eclipse treatment planning system for all dose calculations in this study were the Acuros XB version 10.0.28 and the AAA version 10.0.28. The AAA was originally developed to replace the pencil beam model and to improve the dose calculation accuracy in heterogeneous media. The AAA accounts for the presence of heterogeneities by performing simple density scaling of Monte Carlo derived kernels. Secondary electron transport is only modeled macroscopically. The depth-directed and lateral components are independently scaled. The scaling of the depth-directed component is done by taking into account the radiological distance between the surface and the point of interest, while the scaling of the scatter kernel is done by calculating the water equivalent path length radially from the center of the beamlet. It does not predict accurately the divergent scatter of heterogeneities from upper levels. Detailed description of the AAA can be found in Tillikainen *et al.*[6]

Besides the widely used Monte Carlo method, AXB also belongs to one of the approaches of obtaining open form solution to the LBTE. Monte Carlo method indirectly obtains the solution by following the histories of a large number of particle transports through successive random interactions in media. It produces stochastic errors when insufficient number of particle histories are followed. AXB explicitly solves the LBTE by numerical methods. It can produce systematic errors due to discretization resolution in space, angle, and energy. With sufficient fine-tuning, both methods will converge on the same solution. Detailed description of the AXB can be found in Vassiliev *et al.* and Fogliata *et al.*[8,9]

AXB provides two options of dose reporting modes, i.e., dose-to-water, Dw, and dose-to-medium, Dm. Both calculate the energy-dependent electron fluence based on material properties of the interested media. The process for Dw and

Dm is the same during the AXB transport calculation. The difference between them is mainly in the postprocessing step, during which the energy-dependent fluence resulted from transport calculation is multiplied by different flux-to-dose response functions to obtain the absorbed dose value. AXB uses a medium-based response function for Dm and a water-based response function for Dw. Similar to the Monte Carlo method, the result of Dw is just rescaling that of Dm with the stopping power ratio between the medium and water.[10] The option of Dm was selected for all the AXB calculations in this work.

The dose calculation grid resolution can be set by users from 1 to 5 mm for AAA and from 1 to 3 mm for AXB during the treatment planning. In order to investigate the influence of the calculation resolution of AAA10 and AXB10 for small fields and IMRST treatment plans, all the dose calculations for verifications were taken at both 1.0 mm and 2.5 mm grid resolution for comparison.

II.B. Verification in a rectangular phantom with air cavity

The central axis percentage depth dose data (PDD) of a rectangular phantoms with a $5 \times 5 \times 30$ cm^3 air cavity were taken for 6 MV beam. The air cavity was sandwiched between 5 cm thick of 30×30 cm^2 solid water slabs above and 15 cm thick of solid water slabs below (Gammex-RMI, Middleton, WI). The rectangular air cavity was created by placing two slabs of rectangular perspex slabs between the solid water slabs. These two pieces of perspex located on both lateral sides were only used to support the air cavity. Very small portion or none of the single small fields used in this experiment would irradiate the perspex so its influence to the dose was almost negligible. The axial and sagittal computed tomographic (CT) images located at the center of the air cavity phantom are illustrated in Fig. 1. The central axis PDD was measured using very thin TLDs. The isocenter was set at 1 cm below the distal surface of the air cavity. The field sizes used were 2×2 cm^2, 3×3 cm^2, and 5×5 cm^2. The size of the thin TLD 100 chips (Harshaw, Erlangen, Germany) was 3.2 mm $\times$ 3.2 mm $\times$ 0.381 mm. The sensitivity value for each TLD chip that related its individual dose response to the mean dose response of the selected batch was found so as to improve the accuracy of our measurement. The sensitivity value was taken as the average of three irradiations. The standard deviation, SD, of the sensitivity values of the selected TLD chips over the three irradiation was about 1.5%. In order to reduce statistical errors for the TLD measurement, the PDD measurement by TLD at each depth was repeated four times. The accuracy of the above measurement was the SD of the measured dose over the four irradiations. The measured PDD were then compared with the predicted PDD by AAA10 and AXB10 using both 1.0 mm and 2.5 mm grid resolution. All dose calculations were performed to deliver 2 Gy to the isocenter at 1 cm depth below the air cavity. The dose at each depth was then normalized to the depth of maximum dose along the central axis to generate the PDD. The original CT numbers of the phantom were used for the automatic material assignment in AXB calculation, for

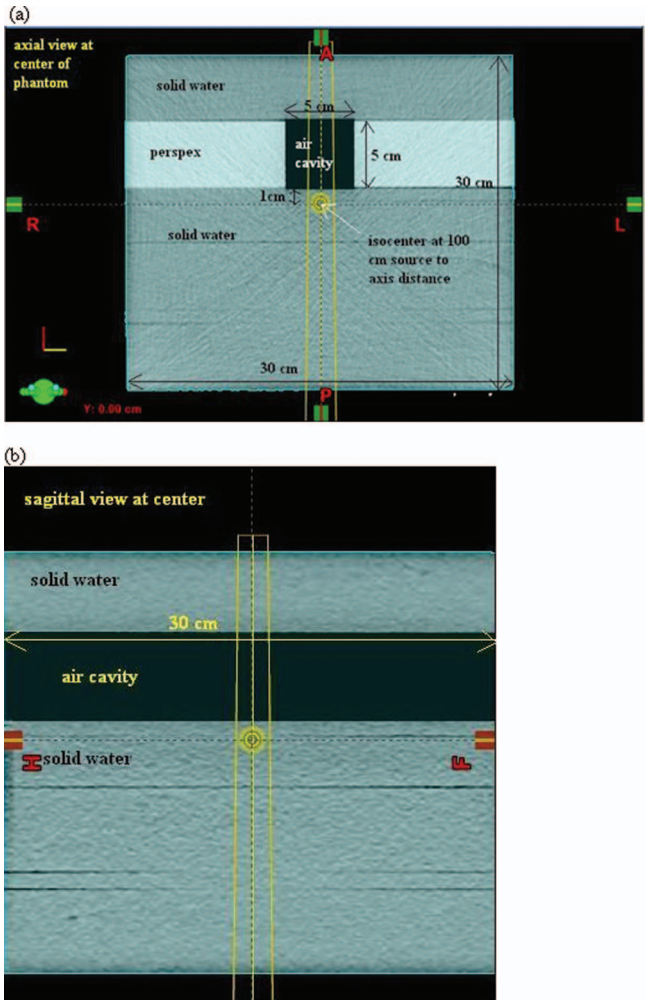

FIG. 1. (a) An axial and (b) sagittal CT image at the center of the simple geometric rectangular phantom containing the air cavity.

which only five biological materials were available, including lung, adipose tissue, muscles, cartilage or bone.

In addition, comparison to the PDD generated by the Monte Carlo simulation was also performed. The Monte Carlo system employed was the parameter reduced electron-step transport algorithm (PRESTA) version of the electron gamma shower (EGS4) computer code. Histories of 2.0×10^8 were followed. The simulation time was shortened by using high cutoff energies. The cutoff energies for electrons and photons were set to be 0.521 MeV and 0.01 MeV, respectively. The standard error of about 2% was achieved. The details of the simulation employed can be found in our previous study.[7]

II.C. Verifications in anthropomorphic phantom with IMSRT setups

The doses near air/tissue interface from five different IMSRT plans were measured in an anthropomorphic phantom (the RANDO phantom, The Phantom Laboratory, Salem, NY). The structure of the original anthropomorphic phantom near the NP region was rather simple, with mainly bone and

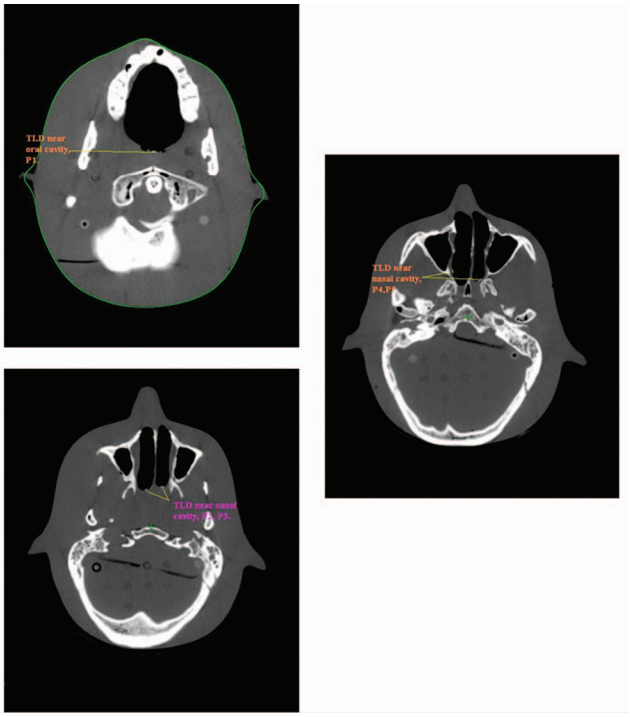

FIG. 2. Three axial CT image showing the positions of the TLDs near air/tissue interfaces in the anthropomorphic phantom.

tissue equivalent materials. The location near the NP region was modified by the authors to simulate that of a typical patient. It included the creation of nasal cavities and recess near the air/tissue interfaces for holding TLD-100 chips (Harshaw, Erlangen, Germany). Four TLD recesses were made near the nasal cavities and one was made near the oral cavity. The CT images showing the position of the TLDs were shown in Fig. 2.

The same planning parameters of five patients previously treated with 7–10 noncoplanar stereotactic intensity modulated fields were used to irradiate the NP region of the anthropomorphic phantom. The beam angles of the original patient plans were chosen based on the beam's eye view to obtain the best coverage of the target volume and best sparing of brain stem and spinal cord. The gantry angles chosen ranged from 125° to 235° in the counterclockwise direction. Posterior or posterior oblique fields that might pass through the base board and head support were not used. At least four to five beams were anterior oblique fields that might pass through air cavities before irradiating the target volume. The beam angle between adjacent fields was at least 30° apart from each other. Usually less than half of the beams were noncoplanar, all of which were anterior oblique fields to avoid gantry couch collision. The jaw sizes used ranged from about 3×3–5×5 cm^2. The location of the isocenter was selected to simulate the actual treatment and cover all the five recesses. For irradiation of the real patients, 18 Gy in three fractions should be given to cover 95% of the PTV. For this TLD measurement, the prescribed doses were reduced to 0.8 Gy per fraction, so that the doses to each TLD could be kept within the linear dose response range. Each TLD was calibrated by irradiating it to a known dose of 1 Gy using 6 MV photon beam at 5 cm depth in a solid water phantom with 100 cm source to phantom distance. Each was also assigned a sensitivity value as mentioned for the previous PDD measurement. The measurement for each patient plan was performed five times and the average values were reported. Dose calculation was then performed for each planning case using both AAA and AXB. All the AXB calculations performed used identical monitor units, jaw settings, and multileaf collimator (MLC) leaf positions as in their corresponding AAA dose calculations. The measured dose data were then compared with the calculated values using both 1.0 mm and 2.5 mm grid resolution. The root-mean-squared errors (RMSE) were reported to summarize the differences between calculated values and measured values of the five points.

II.D. Comparison of dose calculation times

The calculation times of AAA and AXB for both the verification of single field using the simple rectangular phantom and that of the multiple IMSRT fields using the anthropomorphic phantom were also recorded and compared. A standalone Dell T5500 workstation (Dell, Round Rock, TX) with 24 GB RAM and 64-bit Windows XP (Microsoft, Redmond, WA) was used for the dose calculation. AXB provides two options for multiple-field plan, namely, the plan-based calculation and the field-based calculation. The first option calculates the plan as a whole while the second one computes each field separately. The second option was selected in the current study.

II.E. Evaluation of dosimetric impact for clinical cases

Twelve NPC patients with persistent disease previously treated with IMSRT boost were selected for this study. The previous treatments were performed using seven to ten noncoplanar static intensity modulated 6 MV beams delivered to a single isocenter. The target volume of each patient was defined by the oncologist in charge using 1.25 mm thick axial CT images. The PTV included the abnormal soft-tissue mass and/or contrast-enhanced volumes with an addition of 3 mm margin to accommodate patient-up errors and organ motion. The mean PTV was 45.7 cm^3 that ranged from 20.6 to 104.4 cm^3. The delineation of the OARs was also done for the brain stem, spinal cord, optic nerves, optic chiasm, lens, and eyes. Our aim was to deliver a prescribed dose of 18 Gy to at least 95% of the PTV over three fractions. Before the stereotactic boost, the patients were previously treated by a primary radiotherapy with IMRT of 70 Gy. The dose constraints for the OARs therefore depended on the doses received by the previous treatment and determined for individual patient by the oncologist.

The treatment was given twice per week using the Varian-Zmed stereotactic radiotherapy system. A frameless system (Zmed Inc., San Diego, CA) with an impression on a bite tray connected to an array of fiducials was used for immobilization and target localization. The array of fiducials could be tracked and the patient position be adjusted in real time by an

infrared optical system. IMSRT planning was performed with the Eclipse planning system using sliding window technique.

The final dose calculations of the original patient plans were performed by AAA with inhomogeneity correction using 1.0 mm grid resolution. AXB dose calculation using 1.0 mm grid resolution of each plan was performed retrospectively using exactly the same monitor units and MLC leaf movement setting as the corresponding AAA plan. Dose–volume histograms (DVHs) were produced for all plans so that the doses to the PTV and OARs could be analyzed. For the PTV, the maximum dose, minimum dose, the coverage represented by $V_{>95\%}$ (the volume receiving more than 95% of the reference dose), $V_{>100\%}$ and the hot areas represented by $V_{>110\%}$ were reported and compared between the prediction from the two algorithms. For the OARs, the dose encompassing 1% ($D_{1\%}$) and 5% ($D_{5\%}$) of the volumes for brain stem, spinal cord, optic chiasm, optic nerve, and the mean doses to lens were also reported and compared. The plan conformity was evaluated through comparisons using the conformation number, CN, which was defined as the product of $V_{T,ref}/V_T$ and $V_{T,ref}/V_{ref}$, where $V_{T,ref}$ represents the volume of the target receiving a dose equal to or greater than the reference dose; V_T represents the physical volume of the target, and V_{ref} represents the total tissue volume receiving a dose equal to or greater than the reference dose.[15] The reference dose used to compute the CN is the prescription dose. The first ratio assesses quality of target coverage, and the second ratio assesses the amount of healthy tissue being involved in the reference dose. The higher the CN values, the better the conformity. A CN value of 1 represents perfect conformity.

III. RESULTS

III.A. Verification of PDD in the rectangular phantom with air cavity

It is seen from Figs. 3(a) to 3(c) that the Monte Carlo simulated PDD data matched quite closely to the TLD measured PDD. The results from the calculations using AAA are inadequate to predict accurately the secondary build-up at and also the first 1 cm beyond the distal interface between air and solid water from 2 × 2 to 5 × 5 cm^2 fields. If taking the measured data by TLD as the reference (the accuracy of the TLD measurement was about 3%), the PDD measured at the distal air/solid water interface was 16.3%, 23.3%, and 38.2% for the 2 × 2, 3 × 3, and 5 × 5 cm^2 field, respectively, while those predicted by AAA using 1.0 mm grid size ($AAA_{1.0\,mm}$) were 57.1%, 60.0%, and 64.0%, respectively. The overestimation of PDD at the distal interface by $AAA_{1.0\,mm}$ was up to 41% when 2 × 2 cm^2 field was used. On the other hand, significant improvement in predicting the secondary build-up curves by AXB was observed. Overestimations of PDD by AXB were still observed at the distal air/solid water interface. The predicted PDD was 22.5%, 26.7%, and 45.5%, respectively, when using 1.0 mm grid size. The distal interface PDD was overestimated by about 6% for 2 × 2 cm^2 by AXB using 1.0 mm grid size ($AXB_{1.0\,mm}$). However, at depths 2 mm or more beyond the distal interface, the predicted PDD

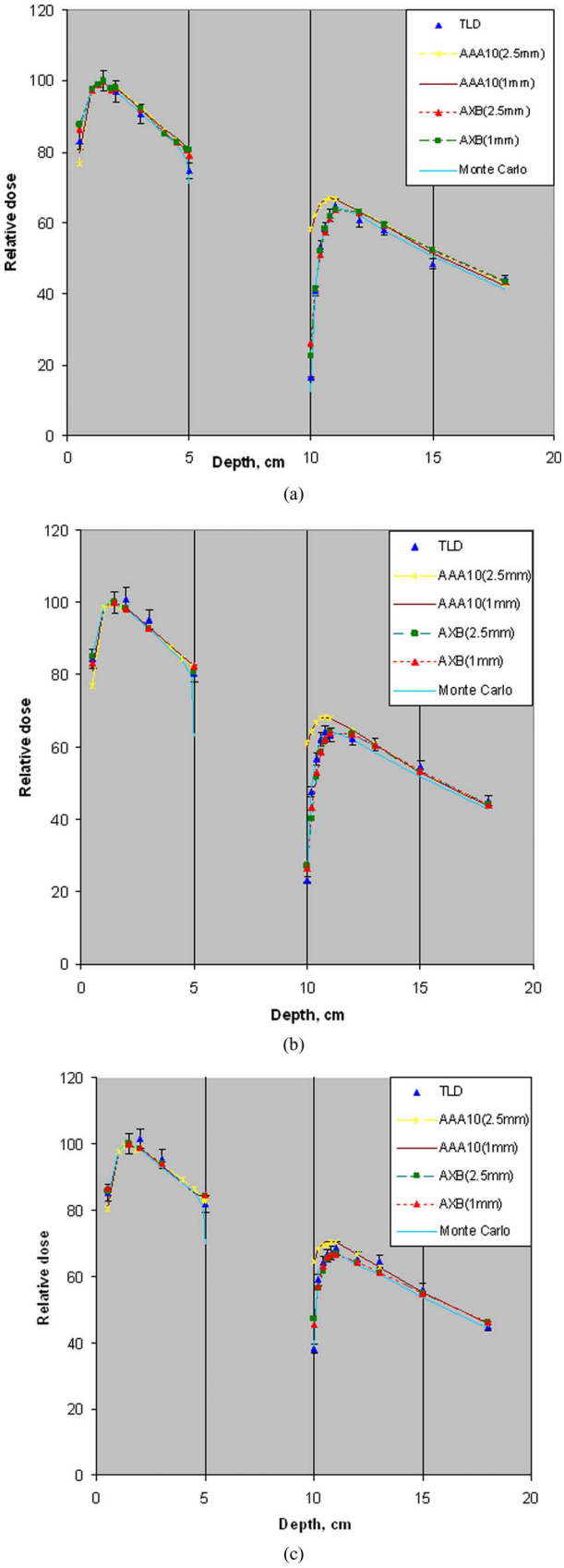

FIG. 3. The predicted percentage depth dose curves predicted by AAA and AXB compared to the measured and Monte Carlo simulated data using the rectangular phantom for (a) 2 × 2 cm^2, (b) 3 × 3 cm^2, and (c) 5 × 5 cm^2 fields. The measured data and Monte Carlo simulated data were from Kan *et al.* (Ref. 7).

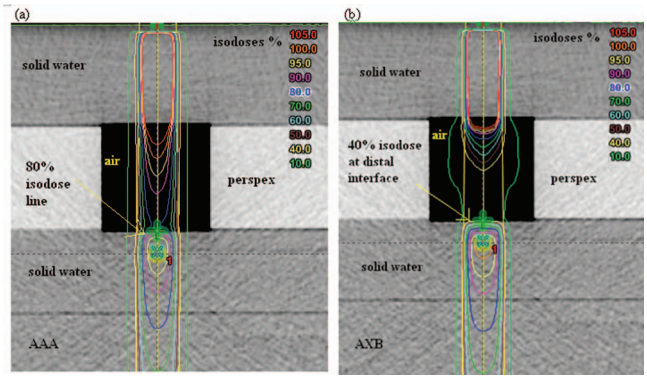

FIG. 4. The isodose distribution calculated by the $AAA_{1.0\,mm}$ and $AXB_{1.0\,mm}$ in the rectangular phantom containing air cavity for a 2×2 cm^2 field 6 MV beam.

by AXB caught up very well with the measured values for all field sizes, while AAA still overestimated the PDD by more than 10% at the first 2–3 mm beyond the air cavity. The overestimation by AAA decreased with depths beyond the air cavity until the peak of the secondary build-up region. Both AAA and AXB predicted negligible build-down effect at the proximal air/solid water interface when compared to the Monte Carlo simulation. Insignificant differences were found between the PDD curves predicted by using 1.0 mm grid and 2.5 mm grid for both algorithms when confined to this simple geometric setup. Figure 4 shows that there was significant difference in the calculated isodose distribution between the $AAA_{1.0\,mm}$ and $AXB_{1.0\,mm}$ in the phantom for a 2×2 cm^2 field. Looking at the dose profiles inside air and near the air-tissue interfaces, the relative doses outside the field edge predicted by AXB were higher and along the central axis were lower than those predicted by AAA.

III.B. Verification of accuracy using IMSRT setup in anthropomorphic phantom

Figures 5(a)–5(e) show the distribution of percentage differences between the measured doses and the doses

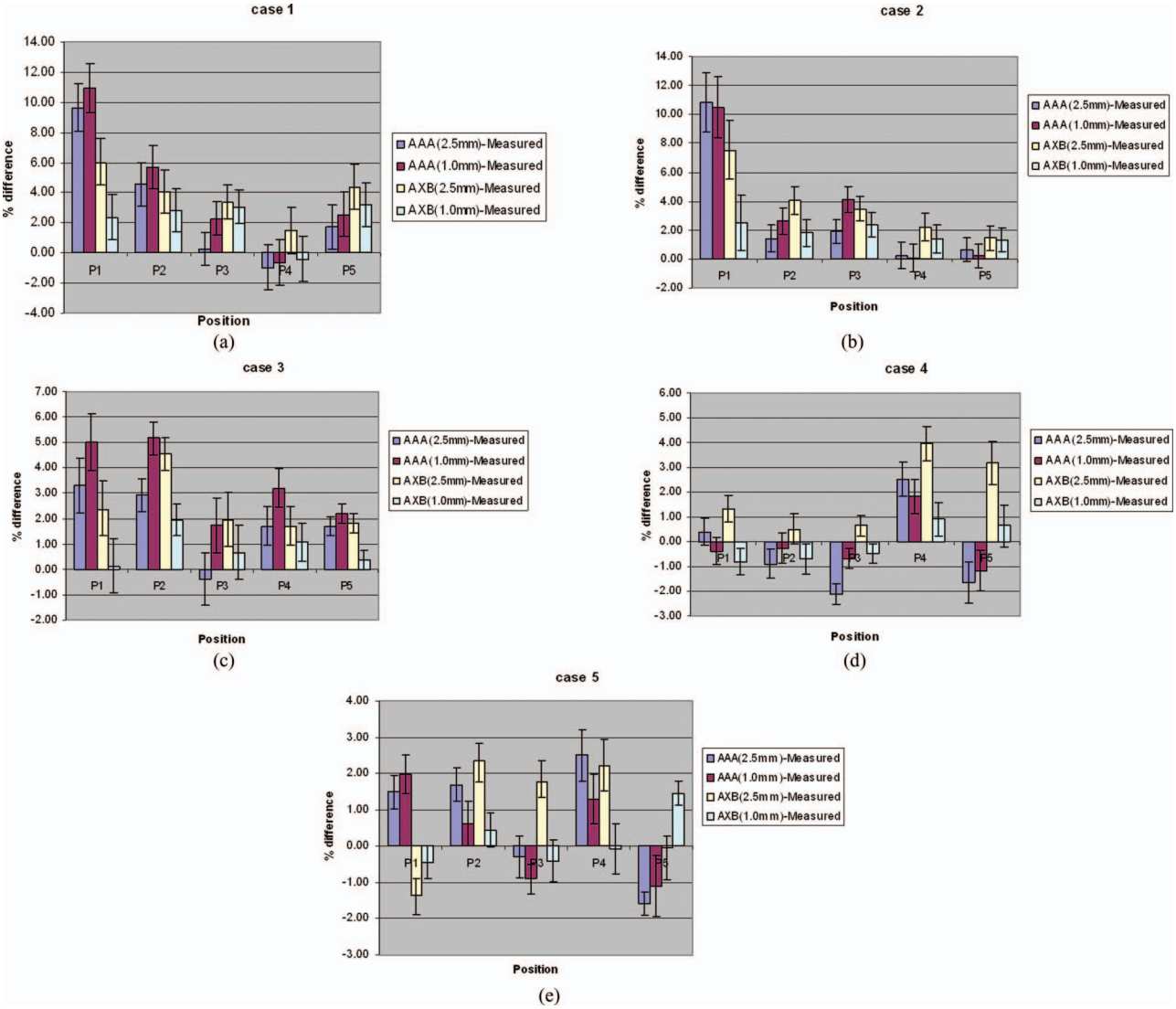

FIG. 5. The distribution of percentage differences between the measured doses and the calculated doses by both AAA and AXB at the five selected points near air/tissue interfaces using the actual IMSRT setup of the selected five cases, (a) case 1, (b) case 2, (c) case 3, (d) case 4, and (e) case 5. The measured doses were taken from Kan *et al.* (Ref. 7).

TABLE I. A summary of the comparison between TLD measured values and calculated values of the five points measured for the five IMSRT plans.

	Root-mean-squared error (RMSE) of the five measured points			
Case number	$AAA_{2.5\,mm}$—measured data[a]	$AAA_{1.0\,mm}$—measured data[a]	$AXB_{2.5\,mm}$—measured data[a]	$AXB_{1.0\,mm}$—measured data[a]
1	4.8	5.7	4.1	2.6
2	5.0	5.2	4.3	1.9
3	2.2	3.7	2.7	1.0
4	1.7	1.0	2.4	0.7
5	1.7	1.3	1.8	0.7

[a]The measured doses were from Kan *et al.* (Ref. 7).

calculated by both AAA and AXB at the five selected points near air/tissue interfaces using the actual IMSRT setup of five patient plans. P1 was located near the air/tissue of the oral cavity, where the width of the air cavity was relatively larger than those of the nasal cavities, as shown in Fig. 2. P2–P5 were located near the air/tissue of the nasal cavities. It can be seen that for most of the time, the AAA algorithm overestimated the doses compared to measurements. This phenomenon was more obvious for P1 from case 1 to case 3. The overestimation of doses was up to around 10% of the measured dose. All the percentage differences predicted by $AXB_{1.0\,mm}$ were within 3% of the measured values. Taking the measured data as the reference doses, Table I shows the summary of the RMSE of the five predicted point doses for AAA and AXB using both 2.5 mm and 1.0 mm grid resolution. It can be seen that the RMSE values ranged from 1.0 to 5.7 for the five cases using $AAA_{1.0\,mm}$, while it only ranged from 0.7 to 2.6 using $AXB_{1.0\,mm}$ grid size, indicating the best match between $AXB_{1.0\,mm}$ and the measured data. By reducing the grid resolution from 2.5 mm to 1.0 mm, significant improvement in dose calculation accuracy was observed for AXB, while negligible improvement was observed for AAA.

III.C. Dosimetric impact on the target coverage and OAR doses of real patients

Table II provides a summary of the PTV coverage, conformity, and OAR doses averaged for the 12 IMSRT patient plans calculated by the $AAA_{1.0\,mm}$ and $AXB_{1.0\,mm}$ algorithms. The coverage of the PTV represented by $V_{>100\%}$ was reduced by 4.1% due to the recalculation from $AAA_{1.0\,mm}$ to $AXB_{1.0\,mm}$. The minimum dose to the PTV was also reduced by 3.7% when using $AXB_{1.0\,mm}$. Negligible differences were found in the target coverage represented by $V_{>95\%}$ and the amount of hot areas represented by $V_{>110\%}$ between them. Very small difference was found in the CN value representing a comparable target dose conformity. Figures 6(a) and 6(b) show the comparison of isodose distribution on two of the axial CT images of a typical patient between $AAA_{1.0\,mm}$ and $AXB_{1.0\,mm}$. This patient plan refers to case 1 used in the anthropomorphic phantom verification of Sec. III.B. It can be seen that the contour of the PTV included some air cavity near the gross tumor volumes. The reduction of the PTV coverage estimated by $AXB_{1.0\,mm}$ in and near the air cavity was clearly shown by the 18 Gy isodose line. It can be observed from Table IV that both $D_{1\%}$ and $D_{5\%}$ to most of the serial organs were slightly reduced when $AXB_{1.0\,mm}$ was used instead of $AAA_{1.0\,mm}$. Although the reduction was mostly statistically significant, the actual difference only ranged from 3% to 6%. The mean doses to the lens were also slightly reduced by using AXB calculation. However, such small reduction of mean doses might not be clinically significant. Figure 7 shows the comparison of the DVH of a typical patient between $AAA_{1.0\,mm}$ and $AXB_{1.0\,mm}$. The DVH curves of the OARs were very close to each other, while slightly inferior target coverage was estimated by $AXB_{1.0\,mm}$ compared to $AAA_{1.0\,mm}$.

TABLE II. Summary of the PTV coverage, conformity, and OAR doses averaged for the 12 SRT boost patient plans calculated by the $AAA_{1.0\,mm}$ and $AXB_{1.0\,mm}$ algorithms.

Parameter	$AAA_{1.0\,mm}$	$AXB_{1.0\,mm}$	*p*-value
	PTV		
Maximum dose	20.8 ± 0.4	21.0 ± 0.4	a[a]
Minimum dose	16.1 ± 1.9	15.5 ± 1.9	a
V > 100%	98.9 ± 1.0	94.8 ± 3.6	a
V > 95%	99.9 ± 0.3	99.6 ± 0.4	–
V > 110%	4.2 ± 1.8	4.1 ± 2.6	–
CN	0.75 ± 0.08	0.73 ± 0.06	–
	OARs		
Brain stem			
D1%	3.3 ± 1.6	3.2 ± 1.5	a
D5%	2.7 ± 1.4	2.6 ± 1.4	a
	Spinal cord		
D1%	1.9 ± 1.3	1.8 ± 1.3	a
D5%	1.6 ± 1.1	1.5 ± 1.1	a
	Optic chiasma		
D1%	1.8 ± 2.7	1.6 ± 2.5	a
D5%	1.3 ± 1.6	1.2 ± 1.5	–
	Lt optic nerve		
D1%	3.1 ± 4.7	3.0 ± 4.6	–
D5%	2.6 ± 3.8	2.5 ± 3.7	a
	Rt optic nerve		
D1%	1.7 ± 1.3	1.6 ± 1.4	a
D5%	1.5 ± 1.1	1.4 ± 1.1	a
	Lt lens		
Mean	0.50 ± 0.48	0.45 ± 0.47	a
	Rt lens		
Mean	0.49 ± 0.46	0.44 ± 0.45	a

[a]The symbol "a" indicates that the difference between AAA and AXB is statistically significant with a *p*-value ≤ 0.05.

III.D. Comparison of dose calculation time

Table III shows the dose calculation time required for the rectangular phantom using one single small field. It can be seen that the calculation time required by $AXB_{2.5\,mm}$ was about 7–10 times of that by $AAA_{2.5\,mm}$, while the calculation time required by $AXB_{1.0\,mm}$ was about 5–12 times that of $AAA_{1.0\,mm}$. The difference increased with field size. Table IV

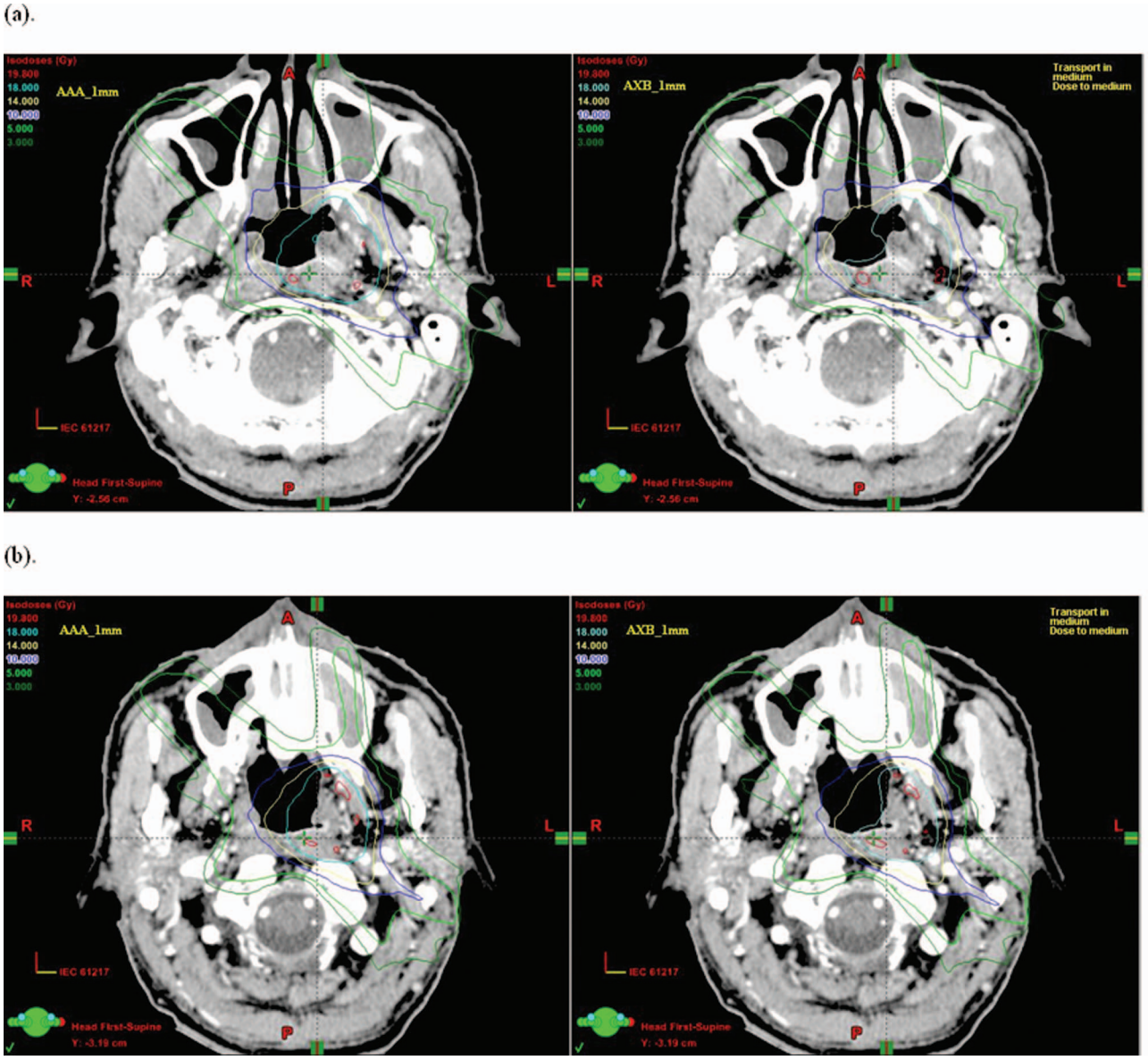

FIG. 6. Side by side comparison of isodose distribution on two of the axial CT images, (a) and (b), of a typical patient (case 1 of Fig. 5) $AAA_{1.0\,mm}$ and $AXB_{1.0\,mm}$.

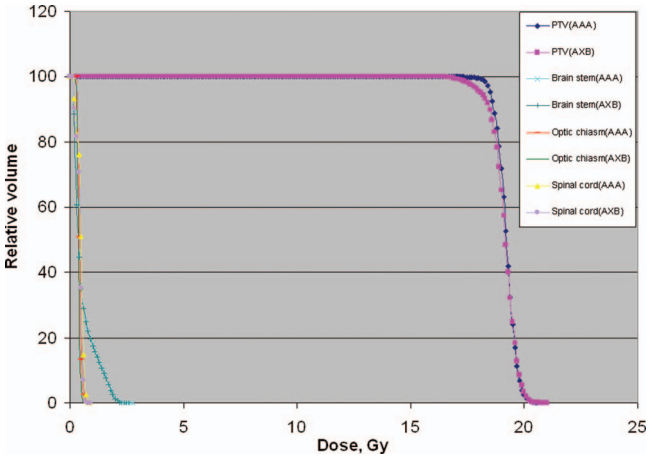

FIG. 7. The comparison of the dose volume histogram (DVH) of a typical patient (case 1 of Fig. 5) between $AAA_{1.0\,mm}$ and $AXB_{1.0\,mm}$.

summarizes the dose calculation time required by the two algorithms for multiple-field IMSRT plans for verification using the anthropomorphic phantom. The dose calculation times required by AXB were more than 20 times of those required by AAA.

TABLE III. Dose calculation times recorded of AAA and AXB from a single field in the rectangular air cavity using the 2.5 mm and 1.0 mm grid resolution.

Field Sizes	Time (s) AAA10 (2.5 mm)	Time (s) AAA10 (1.0 mm)	Time (s) AXB10 (2.5 mm)	Time (s) AXB10 (1.0 mm)
$2 \times 2\ cm^2$	4	23	30	110
$3 \times 3\ cm^2$	5	24	35	140
$5 \times 5\ cm^2$	5	24	52	280

TABLE IV. Dose calculation times recorded of AAA and AXB for IMSRT setup in anthropomorphic of the five cases using the 2.5 mm and 1.0 mm grid resolution.

	Dose calculation time			
Case (no. of fields used)	$AAA_{2.5\ mm}$	$AAA_{1.0\ mm}$	$AXB_{2.5\ mm}$	$AXB_{1.0\ mm}$
1 (7)	15 s	1 min 15 s	5 min 30 s	28 min 35 s
2 (7)	16 s	1 min 27 s	7 min 15 s	44 min 28 s
3 (8)	18 s	1 min 24 s	7 min 12 s	37 min 50 s
4 (8)	23 s	1 min 25 s	6 min 50 s	48 min 40 s
5 (10)	25 s	1 min 58 s	9 min 5 s	46 min 58 s

IV. DISCUSSION

Some previous investigations showed that the AXB, which used a deterministic method to solve the LBTE and was capable of accounting for the specific material composition of the media, would result in improved accuracy of dose calculations in heterogeneous media than the commonly used AAA by comparison against Monte Carlo calculations.[12,13] In our study, the verifications of AXB were performed by comparing the calculated data against experimentally measured data in both rectangular and anthropomorphic phantoms. Since the main interest of this study was to assess dosimetric impact of using the more accurate AXB in IMSRT near the NP region, the verification mainly focused in predicting the dose when small fields were used in presence of air cavity. Detailed verification of the dose accuracy before the dosimetric assessment was essential for us to know whether the AXB was able to provide information regarding the actual doses to target and OARs.

Our results for the rectangular phantom clearly indicated that the use of AXB significantly improved the accuracy under the conditions of electronic disequilibrium compared to AAA. The shape of the secondary build-up curves predicted by AXB, no matter it was using 2.5 mm grid or 1.0 mm grid followed closely to the measured curves. However, the results did not suggest a perfect match. Discrepancies were still observed at the proximal and distal air/tissue interfaces. AXB overestimated the distal air/tissue PDD by about 6% compared to the measured PDD. Those at 2 mm or beyond the interfaces matched well with each other. Although AXB is able to describe the interactions of radiation particles with matter based on approximate numerical methods, it can still produce inaccuracies that result from discretization of the solution variables in space, angle, and energy. Insufficient refinement in variable discretization will produce systematic errors. The degree of inaccuracy depends on the level of sampling of the probability distribution functions applied to the application of variables discretization during explicit LBTE solution. Besides, the achievable accuracy is limited by uncertainties in the particle interaction cross-section data. AXB required the material composition of voxels in the CT image to perform dose calculations. In order to determine the material composition of a given voxel, the values of the Hounsfield unit are converted to mass density using the CT calibration curve. The material can then be determined based on a hard coded look up table in the Varian system database. The automatic material assignment of the current version only confined to five biological materials including lung, adipose tissue, muscles, cartilage or bone. As a result, the accuracy of material assignment and the level of sampling the structure voxels to the calculation grid will also affect the dose calculation accuracy. All the dose calculations performed in this study used the original CT numbers for automatic material assignment. This would lead to the assignment of the solid water and polystyrene slabs to human tissues such as adipose tissues or muscle tissues, and the air cavity to low density lung. Fogliata *et al.* showed that the inclusion of the air material assignment and the provision of better resampling process of the structure voxels to the calculation grid provided by the preclinical version 11.0.03 of AXB provided better agreement with Monte Carlo method than the current clinical version.[12]

On the other hand, AAA could only predict little secondary buildup at regions beyond the air cavity. There were large discrepancies between the AAA predicted and the measured PDD immediately beyond the air cavity. A similar trend was observed by Bush *et al.*, who reported differences of up to 4.5% in the secondary buildup beyond the air between AXB and Monte Carlo calculated results, while it was up to 13% between AAA and Monte Carlo calculated results using a 10 $\times$ 10 cm^2 6 MV beam.[13] For AAA, as already described in detail by Tillikainen *et al.*,[6] heterogeneity was only taken into account by applying density based correction to dose kernels calculated in water. The effect of electron disequilibrium at and near the interfaces between media of different density is approximated by an empirical convolution along a ray line, resulting in the underestimation of the build-up and build-down effects near interfaces in the presence of very low density media like air.

Our verification results in the anthropomorphic phantom have already shown that the dose inaccuracies in doses calculated by both AAA and AXB were significantly reduced when multiple IMRT fields from seven to ten different beam directions were used instead of single field irradiation. This was mainly due to the smearing of errors from different beam directions and segments to the same calculation points. Moreover, the anthropomorphic phantom consists of air cavities that were smaller than that of the single field verification. Overestimation of doses by AAA was still up to 10% near air cavities at some points, especially the one near the oral cavity. Our results based on verification of point doses did not detect any significant differences in dose calculation accuracies by using 1.0 mm grid size compared to 2.5 mm grid size for AAA. However, using AXB with 1.0 mm grid size resulted in significant improvement in the dose accuracies (within 3%) for the five measured points. Smaller grid resolution reduces the averaging effect and leads to better sampling of the structure voxels to the calculation grid. It would allow us to perform a more accurate dosimetric analysis for IMSRT plans. The use of 2.5 mm grid resolution should be avoided whenever possible for stereotactic plans using slice spacing of 1.25 mm.

The dosimetric impact on real patients due to the recalculation from AAA to AXB were investigated for nonsmall-cell

lung and breast cancer treatments.[16,17] For nonsmall-cell lung cancer, the mean dose to the planning target in soft tissue predicted by AXB was found to be 0.4% and 1.7% lower for IMRT and three-dimensional conformal therapy, respectively, while the mean dose to the target in lung tissue was slightly higher (<1%). For the breast cancer, AAA was found to predict a higher dose of 1.6% for the breast target in the muscle tissue compare to AXB, while negligible difference was found in adipose tissue. AAA predicted higher doses than AXB in lung tissue of up to 1.5% for the deep inspiration cases. Our results showed that AAA predicted higher coverage to the planning target volume than AXB in terms of $V_{>100\%}$. For most of the OARs, AXB predicted slightly lower doses. This ensured safe dosages given to the OARs even when the less accurate AAA was used. Regarding the target coverage, the PTV for NPC boost contoured by the oncologists inevitably include some air cavities adjacent to the tumor, especially when 3 mm margin was added to the gross tumor volume. Although separation of air and tissue in PTV was not performed in the dosimetric analysis of this study, by visual examination of the isodose curves of each patient, it was found that the lower doses predicted by AXB mostly occurred in air and/or near the air/tissue interfaces. The target coverage receiving 95% of the reference dose predicted by AXB was very close to that of AAA. On the whole, the lower doses predicted by AXB might not produce significant clinical impact regarding tumor control and complication of OARs. However, the more accurate dosimetric information given by AXB would be useful for the oncologists to have a better understanding of the treatment outcomes.

V. CONCLUSION

Comparisons to experimental measurements and Monte Carlo simulation in the simple geometric phantom showed that the AXB predicted significantly more accurate secondary buildup near and beyond air/tissue interfaces. Comparisons to experimental measurements in the complex anthropomorphic phantoms showed that AXB using dose calculation grid resolution of 1.0 mm was superior in predicting the doses compared to AAA and AXB using 2.5 mm grid. For comparison of 12 real patients with persistent NPC treated using IMSRT, the use of AXB generally showed lower target coverage and lower doses to OARs compared to those calculated from AAA. Our planning criteria of getting 95% of the PTV receiving 100% of the prescribed dose could not be achieved for all 12 patients if AXB using 1.0 mm grid size was used as the reference. It is advisable to use AXB with the 1.0 mm calculation grid as the standard for stereotactic radiotherapy. Whether the inclusion of air cavity inside the PTV is appropriate and how this affects the tumor control probability remains as open questions for oncologist. Our results would be useful for analyzing the treatment outcome and the refining of the treatment protocols when switching from the use of AAA to the more accurate AXB for the future treatment of NPC patients with stereotactic boost.

[a]Author to whom correspondence should be addressed. Electronic mail: kanwkm@ha.org.hk; Telephone: (852) 2990-2776; Fax: (852) 2990-2775.

[1]D. T. Chua, J. S. Sham, P. W. Kwong, K. N. Hung, and L. H. Leung, "Linear accelerator-based stereotactic radiosurgery for limited, locally persistent, and recurrent nasopharyngeal carcinoma: Efficacy and complications," Int. J. Radiat. Oncol. Biol. Phys. **56**, 177–183 (2003).

[2]S. X. Wu, D. Chua, M. L. Deng, C. Zhao, F. Y. Li, J. Sham, H. Wang, Y. Bao, Y. Gao, and Z. Zeng, "Outcome of fractionated stereotactic radiotherapy for 90 patients with locally persistent and recurrent nasopharyngeal carcinoma," Int. J. Radiat. Oncol. Biol. Phys. **69**, 761–769 (2007).

[3]W. Hara, B. Loo, D. Goffinet, S. Chang, J. Adler, H. Pinto, W. Fee, M. Kaplan, N. Fischbein, and Q. Le, "Excellent local control with stereotactic radiotherapy boost after external beam radiotherapy in patients with nasopharyngeal carcinoma," Int. J. Radiat. Oncol. Biol. Phys. **71**, 393–400 (2008).

[4]W. S. Kung, W. C. Wu, K. M. Kam, S. F. Leung, K. H. Yu, Y. K. Ngai, C. F. Wong, and T. K. Chan, "Dosimetric comparison of intensity-modulated stereotactic radiotherapy with other stereotactic techniques for locally recurrent nasopharyngeal carcinoma," Int. J. Radiat. Oncol. Biol. Phys. **79**, 71–79 (2011).

[5]M. Arnfield, C. Siantar, J. Siebers, P. Garmon, L. Cox, and R. Mohan, "The impact of electron transport on the accuracy of computed dose," Med. Phys. **27**, 1266–1273 (2000).

[6]L. Tillikainen, H. Helminen, T. Torsti, S. Siljamaki, J. Alakuijala, J. Pyyry, and W. Ulmer, "A 3D pencil-beam-based superposition algorithm for photon dose calculation in heterogeneous media," Phys. Med. Biol. **53**, 3821–3839 (2008).

[7]W. K. Kan, Y. C. Cheung, H. T. Leung, M. F. Lau, and K. N. Yu, "The accuracy of dose calculations by anisotropic analytical algorithms for stereotactic radiotherapy in nasopharyngeal carcinoma," Phys. Med. Biol. **56**, 397–413 (2011).

[8]O. N. Vassiliev, T. Wareing, J. McGhee, G. Failla, M. Salehpour, and F. Mourtada, "Validation of a new grid based Boltzmann equation solver for dose calculation in radiotherapy with photon beams," Phys. Med. Biol. **55**, 581–598 (2010).

[9]A. Fogliata, G. Nicolini, A. Clivio, E. Vanetti, P. Mancosu, and L. Cozzi, "Dosimetric validation of the Acuros XB advanced dose calculation algorithm: Fundamental characterization in water," Phys. Med. Biol. **56**,1879–1904 (2011).

[10]V. Siebers, P. J. Keall, A. E. Nahum, and R. Mohan, "Converting absorbed dose to medium to absorbed dose to water for Monte Carlo based photon beam dose calculations," Phys. Med. Biol. **45**, 983–995 (2000).

[11]A. Fogliata, G. Nicolini, A. Clivio, E. Vanetti, and L. Cozzi, "Accuracy of Acuros XB and AAA dose calculation for small fields with reference to RapidArc stereotactic treatments," Med. Phys. **38**, 6228–6237 (2011).

[12]A. Fogliata, G. Nicolini, A. Clivio, E. Vanetti, and L. Cozzi, "Dosimetric evaluation of Acuros XB advanced dose calculation algorithm in heterogeneous media," Radiat. Oncol. **6**, 82 (2011).

[13]K. Bush, I. M. Gagne, S. Zavgorodni, W. Ansbacher, and W. Beckham, "Dosimetric validation of Acuros XB with Monte Carlo methods for photon dose calculations," Med. Phys. **38**, 2208–2221 (2011).

[14]C. L. Ong, J. P. Cuijpers, S. Senan, B. J. Slotman, and W. Verbakel, "Impact of the calculation resolution of AAA for small fields and RapisArc treatment plans," Med. Phys. **38**, 4471–4478 (2011).

[15]A. van't Riet, A. C. Mak, M. A. Moerland, L. H. Elders, and W. van der Zee, "A conformation number to quantify the degree of conformality in brachytherapy and external beam irradiation: Application to the prostate." Int. J. Radiat. Oncol. Bio. Phys. **37**, 731–736 (1997).

[16]A. Fogliata, G. Nicolini, A. Clivio, E. Vanetti, and L. Cozzi, "Critical appraisal of Acuros XB and anisotropic analytic algorithm dose calculation in advanced non-small-cell lung cancer treatments," Int. J. Radiat. Oncol. Biol. Phys. **83**, 1587–1595 (2012).

[17]A. Fogliata, G. Nicolini, A. Clivio, E. Vanetti, and L. Cozzi, "On the dosimetric impact of inhomogeneity management in the Acuros XB algorithm for breast treatment," Radiat. Oncol. **6**, 103 (2011).